



24th ABCM International Congress of Mechanical Engineering December 3-8, 2017, Curitiba, PR, Brazil

# COBEM-2017-5950 NUMERICAL SIMULATION OF PARTICULATE FLOW FOR STATIC MUD CAKE PROCESS OVER HETEROGENEOUS POROUS MEDIA

Guilherme Hanauer de Lima Fernando César De Lai Silvio Luiz de Mello Junqueira

Research Center for Rheology and Non-Newtonian Fluids (CERNN), Postgraduate Program in Mechanical and Materials Engineering (PPGEM), Federal University of Technology – Paraná (UTFPR), Curitiba, Brazil. gui\_hanauer@hotmail.com; fernandodelai@utfpr.edu.br; silvio@utfpr.edu.br

Abstract. The lost circulation of drilling fluid, a phenomenon of commonly found in oil industry, occurs whenever the drilling fluid at higher pressure flows from the annulus region towards the porous formation. Besides carrying polymeric particles and fragments of the perforated substrate materials, such flow can also carry solids especially designed to mitigate the lost circulation. In that sense, the walls of the substrate can serve as a filter for the particles carried by the flow and a packed bed of particles may eventually form. In this work, the numerical simulation of the particle flow through a vertical porous channel is performed. The porous substrate is modelled as a macroscopic porous medium, where the solid phase is represented by disconnected cylinders immersed in a water-glycerin solution. An Euler-Lagrange approach given by the combination of the Dense Discrete Phase Model (DDPM) with the Discrete Element Method (DEM), respectively, is applied to the coupled solution of the continuum (fluid) and the discrete phases (particles). Effects of the porous domain permeability, diameter and mass flow rate of the particles over the pressure and the permeability after the particles deposition are investigated. The raise of the injected particles concentration is proportional to the pressure drop and to the growth in the particle bed thickness, reducing the permeability through the medium.

Keywords: Particulate flow, lost circulation, mud cake, heterogeneous porous media, DDPM-DEM.

## 1. INTRODUCTION

Solid, liquid and gaseous phases interacting with each other are seen in oil-generating rocks, commonly represented as a porous substrate. Properties of the porous media, such as permeability and porosity, may vary accordingly to the size of the solid grains, compaction of the rock and also to the interconnectivity of the pores (Falcone *et al.*, 2009).

The lost circulation takes place whenever the pressure inside the wellbore is higher than the pressure of the substrate and the drilling fluid flows towards the formation. Such situation usually elevates the cost of the process Souza *et al.*, 2009). Therefore, the solids carried by the drilling fluid are filtered on the well-formation interface, creating a layer of particles called mud cake. This filtration mechanism is essential for the success of drilling operations, because it mitigates the lost circulation (Darley and Gray, 1988). Different techniques are used to correct and reduce the lost circulation (Civan, 2007).

The purpose of this work is to study the deposition of the particles carried by the flow along the fluid-porous interface and its eventual penetration on the porous layer. In this sense, the mathematical model is implemented in order to simulate numerically the particulate flow through the porous media. To calculate the hydrodynamics interactions between solid and fluid phases, the Dense Discrete Phase Model - DDPM (Popoff and Braun, 2007), coupled with the Discrete Element Method - DEM (Cundall and Strack, 1979), are applied. Pressure drop along the channel and the bed height are monitored for distinct porous domains, particles diameters and solids concentration during the particles injection for the bed formation effect analyses.

# 2. PROBLEM FORMULATION

A schematic representation of the problem geometry (Figure 1) representing the filtration mechanism, in which a heterogeneous porous channel with variable porosity, is presented. The microscopic (heterogeneous) porous substrate (Figure 1.a) is represented by an array of staggered cylinders having different diameters to provide a linear variation of

porosity (Figure 1.c). A particle deposition scheme is shown in Figure 1.(b), where the particles transported by the fluid flowing parallel to the interface deposit on the porous interface developing the mud cake itself.

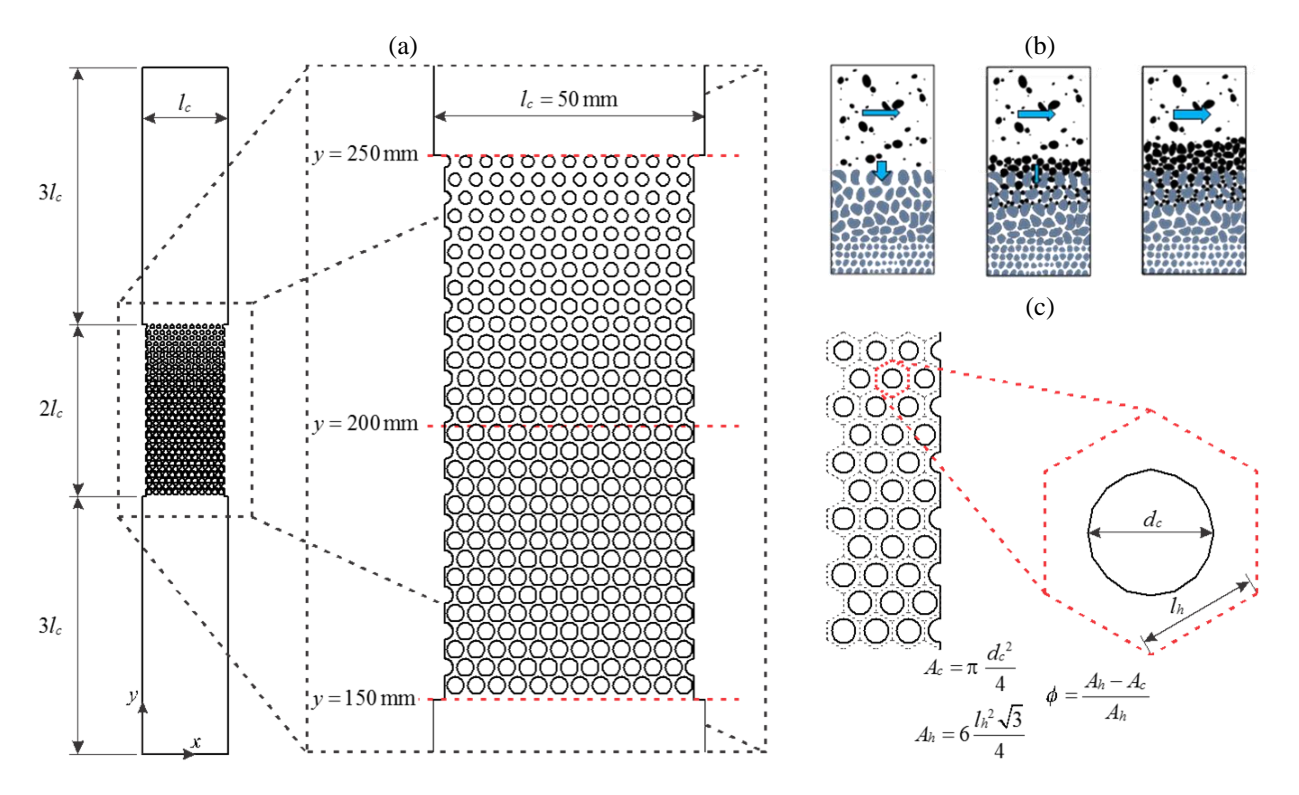


Figure 1. Problem geometry: (a) porous domain in detail, (b) schematic of the mud cake formation process and (c) geometric parameters of the array.

In Figure 1.(a) at the channel upper bound a velocity profile for fully developed flow with average velocity  $U_{\beta,in}$  and pressure  $p_{in}$  is considered. To guarantee the flow through the porous channel a null pressure condition is applied at the other end (y=0).

The channel is considered in the vertical position to favor the formation of a particle bed more evenly distributed along the porous medium, assisting the analysis of the monitor parameters. Injection parameters of particles depends on the diameter of the particles  $d_p$ , of the solids density  $\rho_p$  and the injection surface. It is noteworthy the existence of a pressure gradient due to the null pressure at the channel outlet ( $p_{out} = 0$ ), which provokes the fluid to flow, not only to carry the particles but also provide the eventual solids deposition along the porous medium. The channel has width of  $l_c = 50$  mm, a dimension commonly observed in wellbores annular region that serves to adequate the particles sizes used in this study. Boundary layer effects on the particle trajectory are avoided as the porous region has 2 mm less in each side, compared to the free region (absence of solid particles). The porous region has length of  $h_{mp} = 2l_c$ . Also, the free regions have length of  $3l_c$  to avoid any possible effects of the boundary conditions on the particulate flow in the porous domain. The geometry has thickness of 2 mm in the z direction, normal to the xy plane, to fit the spheres inside the domain. Symmetry conditions are applied on the planes parallel to the xy plane. A linear variation of the porosity, represented by changes in the obstacles diameters, is considered in the porous domain ( $\phi = 0.7$  in  $\phi = 0.7$  in  $\phi = 0.4$  in  $\phi = 0.4$ 

The Lagrangian model adopted to represent the particulate flow is a combination of the Dense Discrete Phase Model – DDPM – and the Discrete Element Method – DEM. The DDPM model accounts the interactions between solid and fluid phases, while the DEM is responsible for solving the particles collisions through the soft spheres approach (Deen *et al.*, 2007).

A Newtonian fluid with constant and uniform properties is considered, for a laminar flow; both the fluid and the solid phases are isothermal; the gravitational force acts in the vertical direction. The particles are perfectly spherical with no rotational motion and the deformations caused by particles collisions are neglected. The trajectory of the particles is calculated through a Lagrangian referential.

Two sets of equations for both the solid (Eqs. 1-2) and the fluid (Eqs. 3-4) phases are considered in the mathematical formulation. The particles tracing is calculated via Newton's second law, where velocity and position are determined by a set of ordinary differential equations expressed in terms of the forces that influence the particles acceleration:

$$m_p \frac{d\mathbf{u}_p}{dt} = \mathbf{F}_d + \mathbf{F}_{gb} + \mathbf{F}_{rg} + \mathbf{F}_{vm} + \mathbf{F}_{ls} + \mathbf{F}_{DEM}$$
(1)

$$\frac{d\mathbf{x}_p}{dt} = \mathbf{u}_p \tag{2}$$

where  $m_p$  represents the particle mass;  $\mathbf{x}_p$  the particle position vector;  $\mathbf{F}_d$  the drag force;  $\mathbf{F}_{gb}$  the sum of the gravity and the buoyancy forces;  $\mathbf{F}_{pg}$  the pressure gradient force;  $\mathbf{F}_{vm}$  the virtual mass force and  $\mathbf{F}_{ls}$  the Saffman lift force. The soft sphere approach is applied to model the forces of particles collision ( $\mathbf{F}_{DEM}$ ). Table 1 shows the expression for each one of these forces.

Table 1. Expressions for the forces acting on the discrete phase of the particles.

Forces	Expressions
Gravitational and buoyance	$\mathbf{F}_{gb} = m_p  rac{oldsymbol{ ho}_p - oldsymbol{ ho}_eta}{oldsymbol{ ho}_p} \mathbf{g}$
Pressure gradient	$\mathbf{F}_{pg} = m_p \frac{\rho_\beta}{\rho_p} \big( \mathbf{u}_\beta \nabla \cdot \mathbf{u}_\beta \big)$
Virtual mass	$\mathbf{F}_{vm} = C_{vm} m_p \frac{\rho_{\beta}}{\rho_p} \frac{D}{Dt} (\mathbf{u}_{\beta} - \mathbf{u}_p)$
Drag	$\mathbf{F}_{d} = \frac{3}{4} \frac{m_{p} \mu_{\beta}}{\rho_{p} D_{p}^{2}} C_{D} R e_{p} \left( \mathbf{u}_{\beta} - \mathbf{u}_{p} \right)$
Saffman lift	$\mathbf{F}_{ls} = C_{ls} m_p \frac{\rho_{\beta}}{\rho_p} (\nabla \times \mathbf{u}_{\beta}) \times (\mathbf{u}_{\beta} - \mathbf{u}_p)$
Collision	$\mathbf{F}_{DEM} = \mathbf{F}_n + \mathbf{F}_t$
Normal	$\mathbf{F}_n = \left(k_n \delta_n + \eta_n \left(\mathbf{u}_{12} \cdot \mathbf{n}_{12}\right)\right) \mathbf{n}_{12}$
Tangential	$\mathbf{F}_{t}=-\mu_{a}\left \mathbf{F}_{n}\right \mathbf{t}_{12}$

The term  $\rho_p$  is the particle density,  $C_D$  is the particle–fluid drag coefficient calculated by Morsi and Alexander (1972) model and  $Re_p = \rho_\beta |\mathbf{u}_\beta - \mathbf{u}_p| d_p / \mu_\beta$  is the particle Reynolds number.  $C_{vm}$  is the virtual mass force coefficient.  $C_{ls}$  is the Saffman lift constant (Li and Ahmadi, 1992).

The collision forces are a combination of normal  $(\mathbf{F}_n)$  and tangential  $(\mathbf{F}_t)$  forces. The normal force is calculated through a spring-dashpot model (Luding, 1998), where k,  $\delta$ ,  $\eta$ ,  $\mathbf{u}_{12}$  and  $\mathbf{n}_{12}$  are respectively, the spring coefficient, the overlap between the particles, the damping coefficient, the relative velocity and the unit normal vector at contact. The tangential force is based on the Coulomb friction equation, where  $\mu_a$  is the friction coefficient and  $\mathbf{t}_{12}$  is the unit tangential vector at contact.

Equations of mass and momentum conservation for the continuous phase (fluid) are expressed respectively by:

$$\frac{\partial \varepsilon_{\beta} \rho_{\beta}}{\partial t} + \nabla \cdot (\varepsilon_{\beta} \rho_{\beta} \mathbf{u}_{\beta}) = 0 \tag{3}$$

$$\frac{\partial \left(\varepsilon_{\beta}\rho_{\beta}u_{\beta}\right)}{\partial t} + \nabla \cdot \left(\varepsilon_{\beta}\rho_{\beta}u_{\beta}u_{\beta}\right) = -\varepsilon_{\beta}\nabla p_{\beta} + \nabla \cdot \left(\varepsilon_{\beta}\mu_{\beta}\nabla \cdot u_{\beta}\right) + \varepsilon_{\beta}\rho_{\beta}\mathbf{g} + \mathbf{F}_{DPM} + \mathbf{S}_{DPM}$$

$$\tag{4}$$

where t is the time,  $\varepsilon_{\beta}$  is the volume fraction of continuum phase,  $u_{\beta}$  is the fluid velocity vector,  $\mathbf{g}$  is the gravity acceleration vector,  $\mathbf{F}_{DPM}$  is the coupling term to exchange momentum due to the interaction of discrete phase forces and  $\mathbf{S}_{DPM}$  is the source term due to displacement of fluid in relation the entrance of particles in a given control volume.

The solution of the coupled balance equations (1-4) is based on the Pressure-Based Solver with a segregated method, through the pressure-velocity PC-SIMPLE algorithm (Vasquez and Ivanov, 2000). An implicitly first order time discretization is employed. The interpolation scheme for the advective terms is the upwind first order and the gradients evaluation are evaluated by the Least Squares Cell-Based method. The Node Based Averaging technique (Apte *et al.*, 2008) through Gaussian kernel function is adopted.

## 3. RESULTS AND DISCUSSION

Preliminary results aiming the verification of the numerical procedure have shown good agreement with the literature. Table 2 shows the comparison of numerical and experimental results of terminal velocity, for particles with  $\rho_p = 2560 kg / m^3$  and  $\rho_p = 7710 kg / m^3$  immersed in water, where is possible to observe a good agreement between both approaches (Mordant and Pinton, 2000).

	$d_p$ (mm)	$u_p  (\mathrm{ms}^{\text{-}1})$		_ E(%)	
$u_p$ (IIIII)		Mordant and Pinton (2000)	Present	- L(70)	
Class montiales	0.5	0.074	0.076	3.378	
Glass particles	1.5	0.218	0.215	1.287	
	1.0	0.383	0.375	2.212	
Steel particles	3.0	0.813	0.792	2.608	
	<i>6</i> 0	1 150	1 120	2 (22	

Table 2. Results of terminal velocity for different particles and diameters immersed in water.

To determine the effect of the particle properties over the formed beds for each the porous media configuration and the injection characteristics, a series of parameters were identified. Results are presented for a fluid with properties of a solution containing 73.7% of glycerin and 26.3% of water at 25°C, with corresponding density of 1.188 g/cm³ and dynamic viscosity of  $2.797 \times 10^{-2}$  Pa.s. A constant Reynolds number equal to Re = 250, resulting in an average velocity of  $U_{\beta,in} = 0.118$  m/s, was considered. Particles density is twice that of the fluid. The standard particles concentration injection is  $\dot{m}_{p,ref}$ , which is varied for  $0.5\dot{m}_{p,ref}$  and  $2\dot{m}_{p,ref}$ . The particle diameters for the simulations were  $d_p = 0.6$ , 0.7 and 0.8 mm. Table 3 summarizes the geometric parameters for the porous plug channel, Table 4 shows the default simulation parameters for the particulate flow through the porous plug channel, and Table 5 is a summary of the injection parameters for particles in the default configuration.

TD 11 2	<b>~</b>		C .1		1	1 1
Table 3.	Geometric	parameters	for the	porous	plug	channel.

Parameter	Symbol	Value	Unit
Channel length	$l_c$	50	mm
Length before the porous media	$l_{a,mp}$	150	mm
Length after the porous media	$l_{d,mp}$	150	mm
Porous media height	$h_{mp}$	100	mm
Porous media width	$l_{mp}$	46	mm
Depth of the porous plug channel	$l_z$	2	mm
Porous media porosity	$\phi$	0.4 - 0.7	_
Number of obstacles per row	N	12 and 16	_

Table 4. Default simulation parameters for the particulate flow through the porous plug channel.

Parameter	Symbol	Value	Unit
Reynolds number	Re	250	_
Fluid dynamic viscosity	$\mu_{eta}$	$2.797 \times 10^{-2}$	Pa.s
Fluid density	$ ho_{eta}$	1188	$kg / m^3$
Particles density	$ ho_p$	2376	$kg / m^3$
Particles diameter	$d_{P}$	0.6 - 0.8	mm
Restitution coefficient	η	0.3	_
Stiffness constant	k	500	_
Discrete phase timestep	$t_p$	$10^{-5}$	S
Continuous phase timestep	$t_{eta}$	$10^{-2}$	S

S

Parameter	Symbol	Value	Unit
Injection position	$h_{ip}$	300	mm
Injection surface length	$l_{ip}$	40	mm
Number of injection points	$n_{ip}$	59	_
Injection velocity	$u_{ip}$	0.118	m/s

Table 5. Injection parameters for particles in the default configuration.

Table 6. Summary of problem variables.

 $\Delta t_{ip}$ 

 $10^{-2}$ 

Injection timestep

Parameters of interest	Numerical experiments realized
Número do obstásulos nor fileiro (N)	N = 12, with no particles.
Número de obstáculos por fileira ( <i>N</i> )	N = 16, with no particles.
	$N = 16$ , $d_p = 0.6 \mathrm{mm}$ , $\rho_p = 1782 \mathrm{kg/m^3}$
Particles density ( $\rho_p$ )	$N = 16$ , $d_p = 0.6 \mathrm{mm}$ , $\rho_p = 2376 \mathrm{kg/m^3}$
	$N = 16$ , $d_p = 0.6 \mathrm{mm}$ , $\rho_p = 2970 \mathrm{kg/m^3}$
	$N = 12$ ; and $N = 16$ , $d_p = 0.6 \mathrm{mm}$
Particles diameter ( $d_p$ )	$N = 12$ ; and $N = 16$ , $d_p = 0.7$ mm
	$N = 12$ ; and $N = 16$ , $d_p = 0.8 \text{mm}$

The injection of particulate material must occur aiming to interfere the least possible on the fluid flow in the channel. Particles are injected through two injection lines, one with 30 points and other with 29, as shown in Figure 2.(a). The points are positioned in a staggered arrange, in order to keep a distance between the particles and the symmetry planes. In Figure 2.(b), 10 particle injection lines, with detail to the mesh between the injection position and the first row of cylindrical obstacles. It is possible to notice that the particles form a parabolic profile, due to the fluid velocity at the position where particles are injected. The velocity field is shown in Figure 2.(c), where is possible to observe that particles negligibly interfere with the flow during the injection.

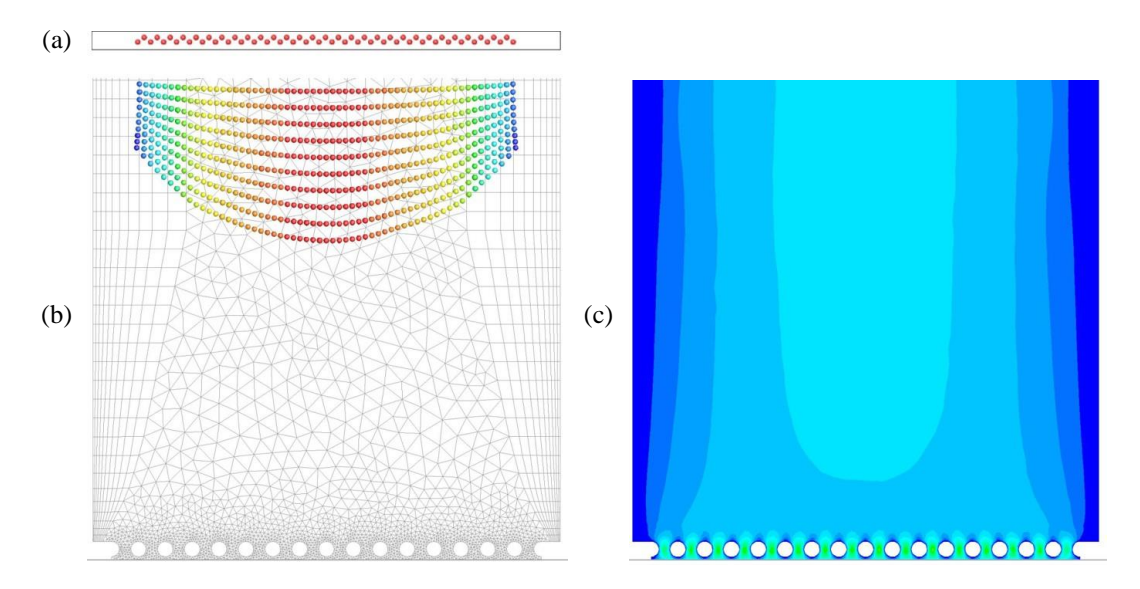


Figure 2. Particle injection process: (a) top view of 59 injection points, (b) mesh detail and particulate injection lines and (c) fluid velocity field.

Two configurations of porous media (Figure 3) are used to investigate the influence of permeability on the packaging of particles, one with 12 obstacles in each row and another with 16. The number of obstructions interferes on the size of the pores, which changes the speed and pressure of the fluid and consequently the permeability. The numerical simulation for the fluid phase flow through the heterogeneous porous plug is performed to obtain the pressure

drop through the porous medium. With the pressure drop results it is possible to find the permeability (K) of the medium through Darcy's law, Equation 5.

$$u_{\beta} = -\frac{K}{\mu_{\beta}} \frac{dp_{\beta}}{dy} = -\frac{K}{\mu_{\beta}} \frac{(p_{\beta}1 - p_{\beta}2)}{(y1 - y2)}$$
 (5)

where  $p_{\beta}1$  is the pressure at  $y=250\,\mathrm{mm}$ ,  $p_{\beta}2$  is the pressure at  $y=150\,\mathrm{mm}$  and  $\mu_{\beta}$  is the viscosity of the fluid. The maximum pressure of the case for N=12 (  $p_{\beta}=1.78\times10^4\,\mathrm{Pa.s}$ ) is the reference pressure (  $p_{ref}$ ) for the calculation of a dimensionless pressure (  $p_{ref}$ ), used in the analysis of other cases.

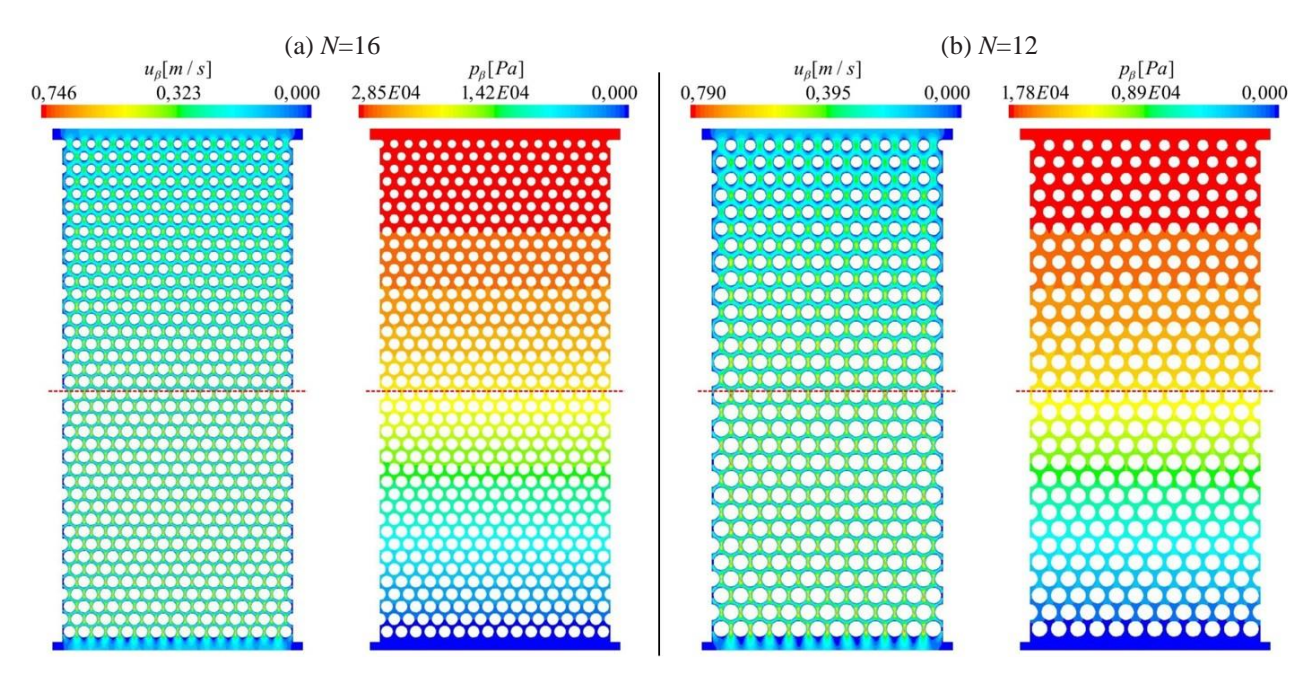


Figure 3. Velocity and pressure fields for the configurations with: (a) N = 16 and (b) N = 12 obstacles.

From the two porous media configurations, the injection of particulate material is performed. In Figure 4 a configuration with  $d_p = 0.6$  mm and N = 16 is used to evaluate the effect of varying the density of the particles. The final particle bed is observed for three cases at the same time ( $t_{ip} = 0.8$ s). In general, there is no great difference between the cases investigated, since a bed with approximately  $h_b = 7.5$  mm of height for the three situations is formed. Regarding the fluid flow, there was also no change in pressure drop and flow velocities for these cases.

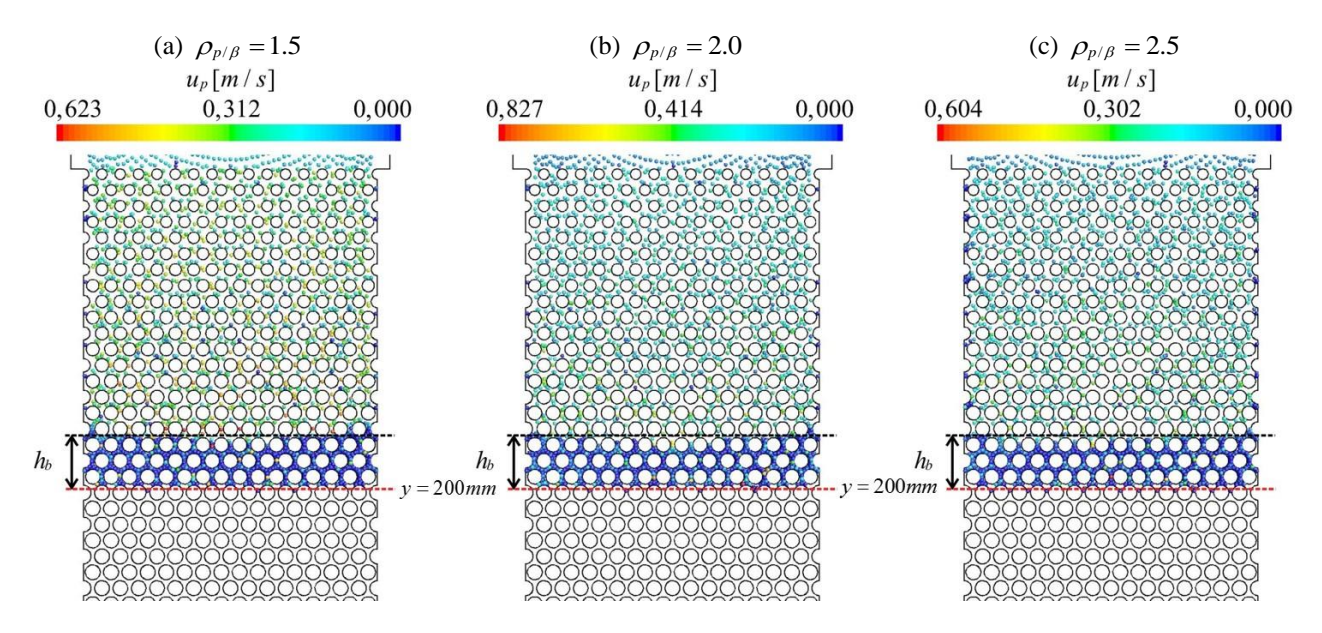


Figure 4. Particle bed height for the variation of the density ratio  $\rho_{p/\beta}$  ( $d_p = 0.6 \,\mathrm{mm}$  and N=16).

Figure 5 presents the results for the injection of particles, considering the porous media with N=16 and N=12 obstacles. It is observed that for N=16 the particles begin to settle in  $y=215\,\mathrm{mm}$ , resulting in a mean bed height of  $h_b=22.5\,\mathrm{mm}$ . For N=12 the deposition position is in  $y=196\,\mathrm{mm}$ , resulting in a bed with  $h_b=23.0\,\mathrm{mm}$ . The beds have similar thickness because particles have the same diameter, but the depth of the particles bed is lower for the medium with larger pore throat.

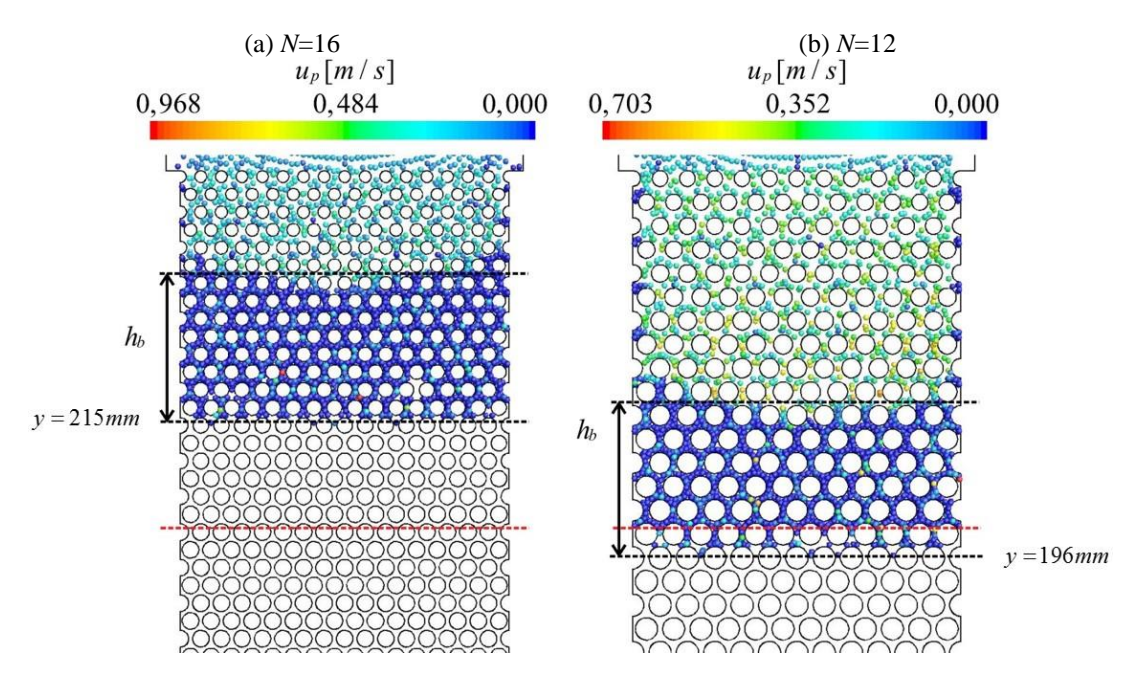


Figure 5. Particle bed height for porous medium variation: (a) N=16 and (b) N=12 for  $d_p=0.8$  mm.

The solids deposition on the porous medium increases the channel pressure drop, promoting the reduction of the permeability of the resulting substrate. For equal injection times, increasing the mass flow rate of injected particles elevates the maximum pressure drop. Furthermore, the same pressure drop for larger injecting particle concentration can be observed at shorter periods. The results for bed height and pressure drop are shown in Table 7.

$t_{ip}[s]$	Particle mass flow rate	N	$d_p[mm]$	$h_b[mm]$	$P_{\beta}$
		16	0.6	4.0	2.05
	$0.5\dot{m}_{p,ref}$	16	0.7	7.5	2.09
	$0.5 m_{p,ref}$	16	0.8	10.0	2.26
		12	0.8	10.0	1.88
		16	0.6	7.5	2.43
0.8	$\dot{m}_{p,ref}$	16	0.7	14.0	2.59
0.8	$m_{p,ref}$	16	0.8	20.5	2.74
		12	0.8	21.0	2.60
		16	0.6	19.0	3.18
	$2\dot{m}_{p,ref}$	16	0.7	30.0	3.40
	$2m_{p,ref}$	16	0.8	41.0	3.62
	12	12	0.8	46.0	3.70

Table 7. Results of  $P_{\beta}$  and  $h_b$  for every investigated case.

It is possible to observe in Figure 6.(a) a synthesis of concentration variation effect for cases with particle diameter of  $d_p = 0.6$ ; 0.7 and 0.8 mm for N = 16 obstacles per row. In this figure it can be noted that for configurations with constant particle diameter there is a raise in the pressure drop when increasing the flow mass flow rate of particles injected, during the whole analyzed injection time, for every configuration. Additionally, it is possible to see that for same mass flow rate, pressure drop is higher for bigger particle diameter.

Figure 6.(b) shows the comparison results between cases with  $d_p = 0.8$  mm for different particle mass flow rate and porous media configuration. It can be observed that for cases with lower obstacles per row the maximum pressure drop in the channel are higher until there is no particle deposition. The increment in particle mass flow rate promotes higher maximum pressure drop at the end of the analyzed injection time. Furthermore, it is possible to see that even for more

permeable porous media configurations (N = 12), cases with higher particle mass flow rate result in structures with similar pressure drop, due to alike bed heights.

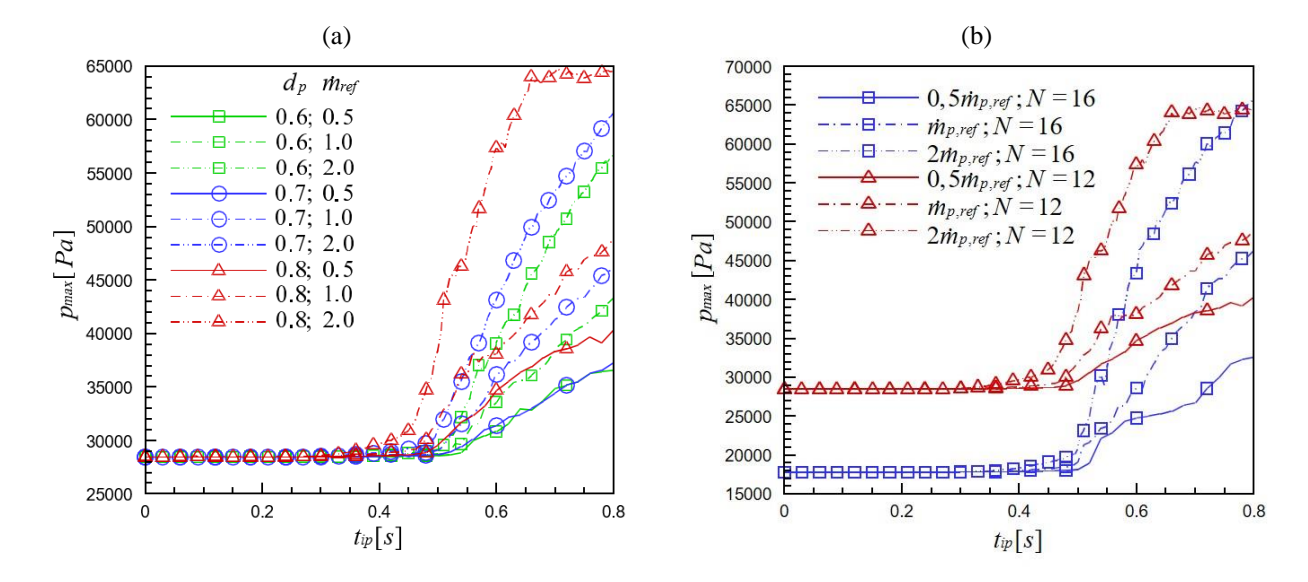


Figure 6. Particle mass flow rate ( $\dot{m}_{p,ref}$ ) variation effect over maximum pressure in the channel along injection time ( $t_{ip}$ ) for cases with: (a) particle diameter  $d_p = 0.6$ ; 0.7 and 0.8 mm (N=16) and (b) obstacles per row N=16 and 12 ( $d_p = 0.8$  mm).

Figure 7 shows the results for configurations where the particles were retained by the porous substrate; colors represent the particles velocities. Effects of different injection rate  $(\dot{m}_{p,ref})$  over the particle bed thickness  $(h_b)$  for different numbers of obstacles per row (N) are displayed. Porous medium with N=12 obstacles per row retains only particles with diameter  $d_p = 0.8$  mm. Cases in which the distance between obstacles is greater than particles diameters of  $d_p = 0.6$  and 0.7 mm, no bed formation is observed.

A correlation was obtained through the least squares method ( $R^2 = 0.966$ ), expressed in Equation (6). The variables used in the calculation of the dimensionless pressure are the number of obstacles (N), the value multiplying the reference concentration of particles in the injection ( $\dot{m}_{p,ref}$ ) and the diameter of the injected particles ( $d_p$ ).

$$P_{\beta} = 5.788 \times 10^{-3} + 9.475 \times 10^{-5} N + 0.973 \dot{m}_p + 2.305 d_p$$
(6)

The variation of the non-dimensional pressure in the channel ( $P_{\beta} = p / p_{ref}$ ) over the particle mass flow rate ( $\dot{m}_p$ ) is presented in Figure 8, for numerical simulation and correlation expression comparison, where the reference value ( $p_{ref}$ ) is the 12 obstacles pressure drop configuration. All simulations were performed for the same injection time ( $t_{ip} = 0.8$  s).

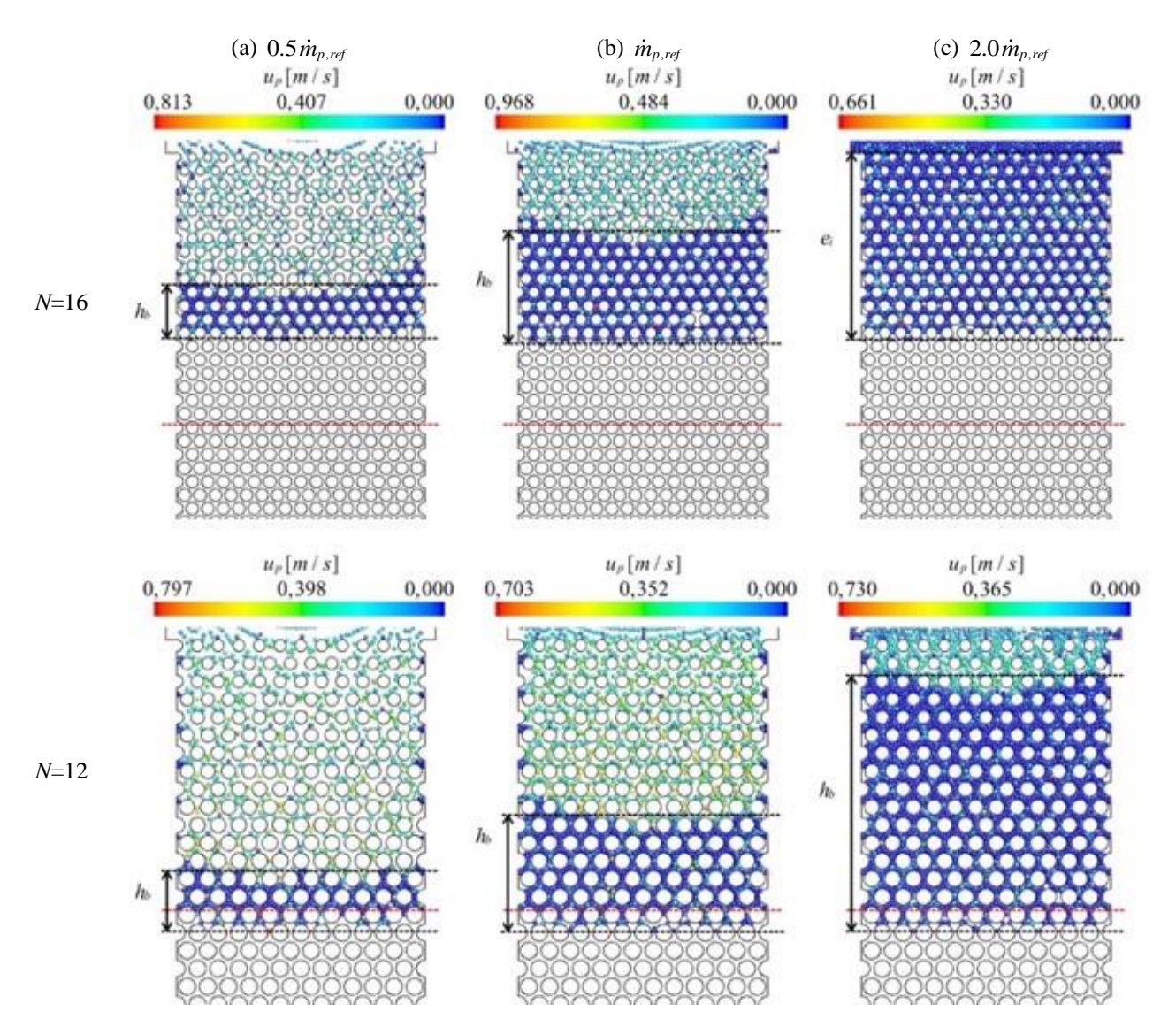


Figure 7. Bed height comparison colored by particles velocity for the cases with particles retention ( $d_p = 0.8 \text{ mm}$ ).

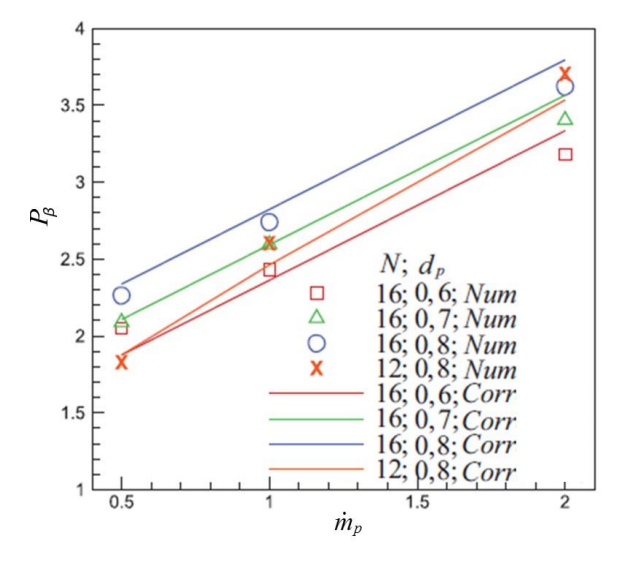


Figure 8. Variation of the dimensionless pressure for the numerical results in comparison to the results obtained through the numerical correlation.

## 4. CONCLUSIONS

In the present study, the particle flow through a vertical heterogeneous porous channel is numerically simulated. The Dense Discrete Phase Model (DDPM) and Discrete Element Method (DEM) are applied to model the fluid and the solid phases. The numerical model is verified through problems found in the literature, where the results show that the physical phenomena of the particulate flow are well represented. The deposition process on porous domain is analyzed by altering characteristic parameters of the problem, such as porous media configuration, particle diameter and particle mass flow rate. Results show the appearance of some patterns, such as those in which the retention and deposition of particles with bigger diameters in upper positions on the porous substrate. The greater the injection time and the particle mass flow rate, the greater will be the height the particle bed. While the increase of the particulate mass flow rate increases of the channel pressure drop, the time for a certain value of pressure drop to be achieved is reduced.

#### 5. ACKNOWLEDGEMENTS

The authors would like to acknowledge the support of IRF/CENPES/PETROBRAS, the PRH-ANP/MCT program (PRH10-UTFPR) and the National Council for Scientific and Technological Development (CNPq).

#### 6. REFERENCES

Apte, S.V., Mahesh, K.; Lundgren, L., 2008. "Accounting for finite-size effects in simulations of dispersed particleladen flows". Int. J. Multiphase Flow, Vol. 34, No. 3, pp. 260-271.

ANSYS, 2015. ANSYS Documentation. ANSYS Inc., Canonsburg, PA.

Civan, F., 2007. "Reservoir formation damage". Gulf Professional Publishing.

Cundall, P.A.; Strack, O.D.L., 1979. "A discrete numerical model for granular assemblies". Géotchnique, Vol. 29, No. 1, pp. 47–65.

Darley, H. C.; Gray, G. R., 1988. "Composition and properties of drilling and completion fluids". Gulf Professional Publishing.

Deen, N.; Annaland, M.V.S.; Hoef, M. Van der; Kuipers, J., 2007. "Review of discrete particle modeling of fluidized beds". Chemical Engineering Science, Elsevier, Vol. 62, n. 1, p. 28–44.

Falcone, G.; Hewitt, G.F.; Alimonti, C., 2009. "Multiphase flow metering". Elsevier.

Goharzadeh, A.; Khalili, A.; Jørgensen, B.B., 2005. "Transition layer thickness at a fluidporous interface". Physics of Fluids (1994-present), AIP Publishing, Vol. 17, n. 5, p. 057102.

Li, A. and Ahmadi, G., 1992. "Dispersion and Deposition of Spherical Particles from Point Sources in a Turbulent Channel Flow". Aerosol Science and Technology, Vol. 16, pp. 209–226.

Luding, S., 1998. "Collisions & Contacts between two particles". In: Physics of dry granular media. Kluwer Academic Publishers, Dordrecht, 1st edition.

Mordant, N.; Pinton, J.F., 2000. "Velocity measurement of a settling sphere". *Eur. Phys. J. B*, Vol. 18, pp. 343–352. Morsi, S.A. and Alexander, A.J., 1972. "An Investigation of Particle Trajectories in Two-Phase Flow Systems". Journal of Fluid Mechanics, Vol. 55, No. 2, pp. 193-208.

Popoff, B.; Braun, M., 2007. "A Lagrangian Approach to Dense Particulate Flows". In International Conference on Multiphase Flow, Leipzig, Germany.

Souza, J.Z.; Ribeiro, D.C.; Fontes, C.E.; Martins, A.L.; Waldmann, A.T.A, 2009. "Análise do escoamento de fluidos particulados durante a perfuração de reservatórios de petróleo". In: III Encontro Nacional de Hidráulica de poços.

Vasquez, S.A.; Ivanov, V.A., 2000. "A phase coupled method for solving multiphase problems on unstructured meshes". In Proceedings of the ASME 2000 Fluids engineering Division Summer Meeting, Boston.

# 7. RESPONSIBILITY NOTICE

The authors are the only responsible for the printed material included in this paper.